J. Fluid Mech. (2003), *vol.* 490, *pp.* 1–14.
DOI: 10.1017/S0022112003005093 Printed in the United Kingdom

Shock wave formation in droplet impact on a rigid surface: lateral liquid motion and multiple wave structure in the contact line region

By K. K. HALLER[1], D. POULIKAKOS[1]†, Y. VENTIKOS[1] AND P. MONKEWITZ[2]

[1]Laboratory of Thermodynamics in Emerging Technologies, Swiss Federal Institute of Technology Zurich, Sonneggstr. 3, CH-8092 Zurich, Switzerland

[2]Ecole Polytechnique Fédérale de Lausanne, Fluid Mechanics Laboratory, CH-1015 Lausanne, Switzerland

(Received 2 July 2002 and in revised form 25 February 2003)

The early phase of high-speed liquid droplet impact on a rigid wall is characterized by compressibility effects through the creation of a shock wave attached to the contact area periphery. Initially, the area of compressed liquid is assumed to be bounded by the shock envelope, which propagates both laterally and upwardly into the bulk of the liquid. In this paper, an analytical model accounting for the lateral liquid motion in the compressed area is developed and compared to the axisymmetric numerical solution of the inviscid (Euler) flow equations. It is shown that the often employed assumption that the compressed area is separated from the liquid bulk by a single shock wave attached to the contact line breaks down and results in an anomaly. This anomaly emerges prior to the time when the shock wave departs from the contact line, initiating lateral liquid jetting. In order to remove this anomaly, the analytical model presented in this paper proposes the transition from a single to a multiple wave structure in the contact line region, prior to jetting eruption. The occurrence of this more complex multiple wave structure is also supported by the numerical results.

1. Introduction

The fluid mechanics of liquid droplet impact on surfaces is of importance to a variety of technological applications such as thermal spray coating, spray cooling, cleaning of surfaces, processing and cutting of materials and ink-jet printing. It is also of fundamental interest, since it involves more general physical phenomena, such as the interaction of shock and expansion waves with each other and with a free surface, as well as jetting eruption. The fluid flow associated with high-speed impinging droplets is rather complicated and still not fully understood (Rein 1993).

During the first stage of droplet impact, the shock wave remains attached to the contact line, as depicted in figure 1(*a*). An analytical study in the acoustic limit, where the shock velocity was assumed to be equal to the ambient liquid speed of sound, has been developed by Lesser (1981). Figure 1(*b*) shows the construction of the shock front as an envelope of all individual wavelets emitted by the expanding contact line. For high impact velocities (a water droplet of diameter 200 μm and velocity of 500 m s^{-1}

† Author to whom correspondence should be addressed: dimos.poulikakos@ethz.ch

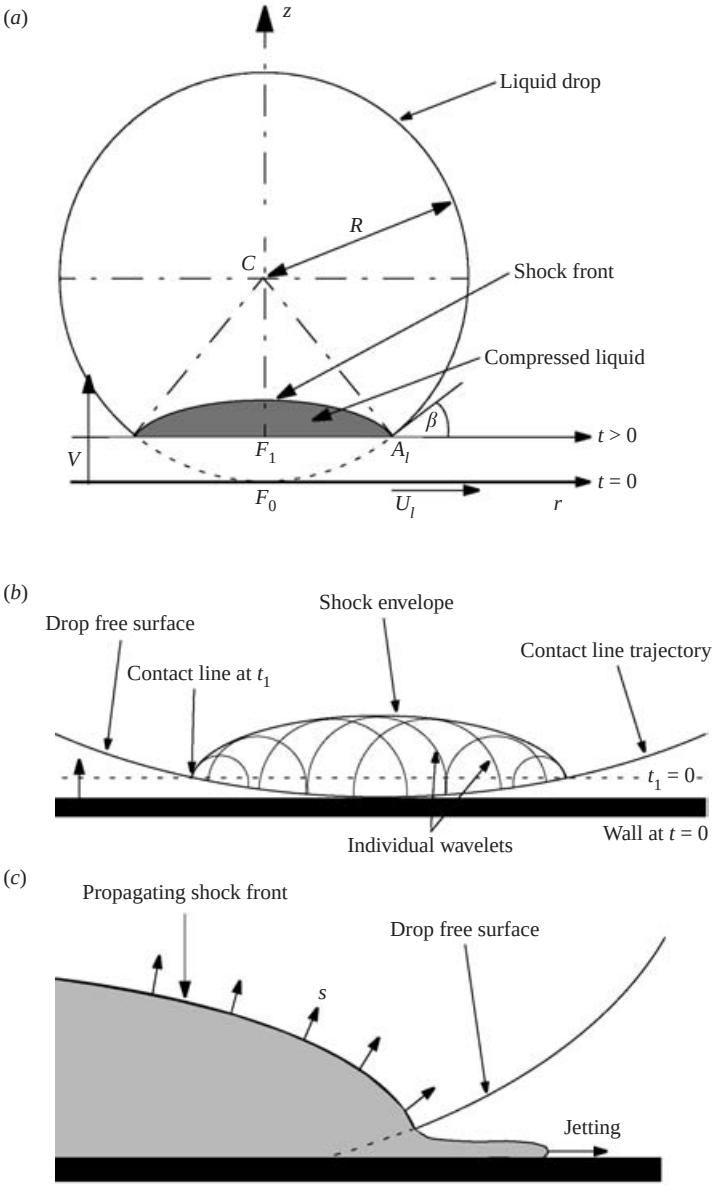

FIGURE 1. (*a*) Droplet impact and creation of the shock wave. (*b*) Construction of the shock front as the envelope of individual wavelets emitted by the expanding contact line. (*c*) Propagation of the shock front: shock wave overtakes the contact line and the jetting commences.

is used as a numerical example throughout this study), the shock speed will be significantly higher than the speed of sound, as shown in Haller *et al.* (2002).

The 'jetting time' is defined as the time when the liquid medium breaks (spalls) through the droplet free surface at the contact line, figure 1(*c*). From a theoretical consideration, this can be expected to occur when the contact line velocity becomes equal to the shock velocity at the contact line. It is well-known that the time characterizing the onset of jetting, obtained by theoretical considerations, is lower

than observed in experiments, see Lesser & Field (1974, 1983), Field, Lesser & Dear (1985) and Field, Dear & Ogren (1989). In this last paper, a speculative explanation of a possible delay of experimental jetting observation is discussed. The major objective of the present work is to investigate the conditions in the contact line region prior to jetting eruption. The issue of jetting eruption and propagation of shock and expansion waves beyond the moment of jetting initiation has been addressed by Haller *et al.* (2002).

In this study, the Reynolds number, $Re = \rho_0 RV/\nu$, is of the order of 50 000. The symbol ν represents the kinematic viscosity of water. This high Re value implies inertia-dominated phenomena and supports an inviscid approach to the problem. A similar comment is valid regarding the importance of surface tension to the impact process. The Weber number ($We = \rho RV^2/\sigma$, where σ is the surface tension coefficient) is estimated to be of the order of 350 000, justifying the assumption that surface tension effect can be neglected. The moment of the shock detachment at the contact line, as well as the effect of viscous forces on droplet impact, has been analysed by Korobkin (1992) and Korobkin & Pukhnachov (1988).

2. The exact solution of droplet impact; geometrical considerations and construction of the shock envelope

The position and radial velocity of the contact line (A_l and U_l in figure 1) are entirely geometrical features of the impact, and can be obtained by considering the impact plane sweeping over the undisturbed drop profile. In order to find the relation for the shock velocity we consider the wave propagation at the contact line.

We assume a spherical droplet geometry. In order to find the coordinates of the contact line, we proceed as follows (cf. figure 1*a*). Since $\overline{F_0F_1} = Vt$ and $\overline{CF_0} = R$, we find

$$\overline{CF_1} = \overline{CF_0} - \overline{F_0F_1} = R - Vt.$$

The x-coordinate X_l of the contact line is determined from the triangle CA_lF_1:

$$X_l = \overline{F_1A_l} = \sqrt{2RVt - V^2t^2}. \tag{1}$$

A derivative with respect to time t yields the radial component of the contact line velocity U_l,

$$U_l = \dot{X}_l = \frac{V(R - Vt)}{\sqrt{2RVt - V^2t^2}}. \tag{2}$$

By the Huyghens principle, at each instant the expanding contact line will emit a wavelet travelling with the shock speed s, figure 1(*b*). In Lesser (1981) this shock velocity was regarded as constant and equal to the ambient speed of sound. As numerically shown by Haller *et al.* (2002) for the case of high-velocity droplet impact, the initial velocity of the individual wavelets is significantly higher than the ambient speed of sound. Therefore, it must be treated as equation-of-state dependent. Moreover, the initial shock velocity is not a constant, rather it increases as the contact line propagates outwards.

We set time $t = 0$ as the time of impact. The z-component of the fluid particle velocity in the compressed region adjacent to the propagating contact line is equal to the wall velocity, i.e. $u\cos\beta = V$. Here, β is the angle between the shock wave and the plane wall, as depicted in figure 1(*a*). The envelope of the shock front at the contact line is constructed from the following consideration. The spherical shock front, emitted at the time instant t, has travelled a distance $s\mathrm{d}t$ at the time $t + \mathrm{d}t$.

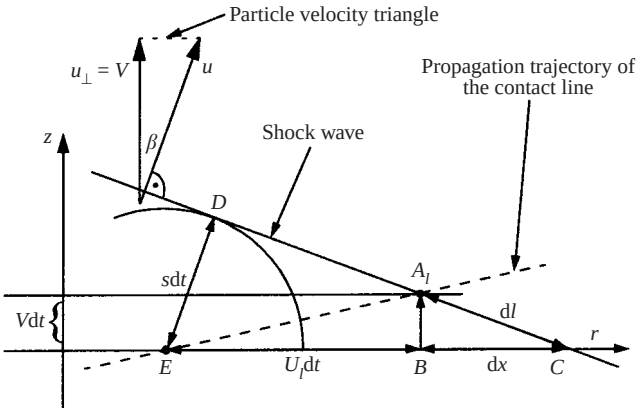

FIGURE 2. Geometrical construction of the shock profile attached to the contact line.

During the same time interval, the contact line moves radially by $U_l\,\mathrm{d}t$ and vertically by $V\,\mathrm{d}t$. The trajectory of the contact line is shown by the dashed line in figure 2 (see also figure 1*b*). Each point of the shock envelope boundary in figure 2 is determined by a tangent from the new contact line position to the circular wavelet of radius $s\,\mathrm{d}t$. This tangent is extended to its intersection with the wall at time t. Employing similarity of triangles ECD and A_lCB, shown in figure 2, yields

$$\frac{U_l\mathrm{d}t + \mathrm{d}x}{s\,\mathrm{d}t} = \frac{\sqrt{(V\,\mathrm{d}t)^2 + \mathrm{d}x^2}}{V\,\mathrm{d}t}. \tag{3}$$

It is convenient to introduce the velocity a as

$$a = \mathrm{d}x/\mathrm{d}t. \tag{4}$$

Equation (3) reduces to

$$a^2(s^2 - V^2) - 2aU_lV^2 + \left(s^2 - U_l^2\right)V^2 = 0. \tag{5}$$

After solving for a, we obtain the usual two solutions of a quadratic equation. Only the solution with the positive sign before the square root has a physical meaning. It can be easily shown that the other solution (with the negative sign before the square root) yields a physically unacceptable value $a < 0$ in the limit $U_l \to \infty$ (the initial moment of impact, $t \to 0$). Based on these considerations,

$$a = \left(U_lV^2 + Vs\sqrt{U_l^2 + V^2 - s^2}\right)/(s^2 - V^2). \tag{6}$$

Next, we employ the well-known consequence of the Euler equations that the liquid particle velocity (jump) u is normal to the shock wave. The similarity of triangle A_lCB and the particle velocity triangle (depicted in figure 2) yields

$$\frac{u}{u_\perp} = \frac{\mathrm{d}l}{\mathrm{d}x} = \frac{\mathrm{d}l}{a\,\mathrm{d}t}, \tag{7}$$

where $u_\perp$ is the component of u normal to the wall. Relation (7) can be rearranged as

$$\frac{\mathrm{d}l}{\mathrm{d}t} = a\frac{u}{u_\perp} = a\frac{u}{V}. \tag{8}$$

In equation (8), we used the condition valid at the wall, $u_\perp = V$. Next, from the similarity of the particle velocity triangle and triangle *ECD*, figure 2, it follows that

$$\frac{\mathrm{d}l}{V\,\mathrm{d}t} = \frac{U_l\,\mathrm{d}t + \mathrm{d}x}{s\,\mathrm{d}t}, \tag{9}$$

which can be rewritten as

$$\frac{\mathrm{d}l}{\mathrm{d}t} = V\frac{U_l + a}{s}. \tag{10}$$

The left-hand sides of equations (8) and (10) are equal, thus

$$a\frac{u}{V} = V\frac{U_l + a}{s}. \tag{11}$$

Solving for the particle velocity u yields

$$u(s) = \frac{V^2}{s}\left(1 + \frac{U_l}{a}\right). \tag{12}$$

Finally, after substitution of velocity a from (6) into (12)

$$u(s) = V\left(s + V\sqrt{1 - \frac{s^2 - V^2}{U_l^2}}\right)\Bigg/\left(V + s\sqrt{1 - \frac{s^2 - V^2}{U_l^2}}\right). \tag{13}$$

If solved for the contact line velocity, equation (13) simplifies to

$$U_l(s) = \pm\frac{su(s) - V^2}{\sqrt{u(s)^2 - V^2}}. \tag{14}$$

For a given value of the contact line velocity U_l, equation (14) contains two unknown variables, namely, s and u. An additional piece of information for the relation between s and u is needed to decide which of the two roots in (14) is meaningful. This is the topic of the next section.

3. The propagation of the shock wave

3.1. *Analytical solution*

The relation between the shock velocity s and the liquid particle velocity u, can be derived from the equation of state when satisfying the Rankine–Hugoniot relations. The locus of possible final states due to the shock compression for a fluid initially at normal density and pressure and zero mass velocity is termed as the principal Hugoniot. For most fluids, it can be expressed over a considerable pressure range by a simple linear relationship (see Heymann 1969 and Lesser & Field 1983):

$$s = s_0 + ku. \tag{15}$$

The symbol s_0 does not always correspond to the speed of sound under ambient conditions. In this study, we apply the fit data $s_0 = 1647\,\mathrm{m\,s^{-1}}$ and $k = 1.921$ (Cocchi & Saurel 1997).

The linear Hugoniot equation (15) is combined with (14) to eliminate the particle velocity u:

$$U_l = \pm\frac{s(s - s_0) - kV^2}{\sqrt{(s - s_0)^2 - k^2V^2}}. \tag{16}$$

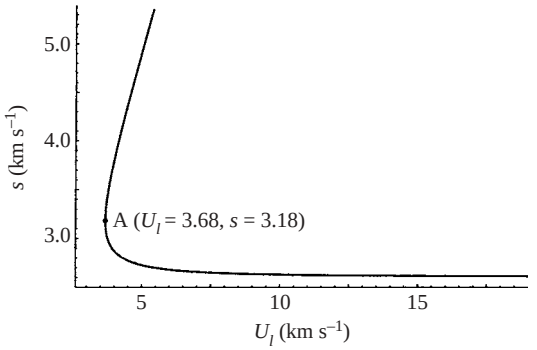

FIGURE 3. Shock velocity vs. contact line velocity for the linear Hugoniot fit.

The physically acceptable solution in our coordinate system is the one which yields a positive contact line velocity. This is determined as follows. The total particle velocity u is higher than the wall velocity,

$$u = |V\hat{z} + u_r\hat{r}| > V. \tag{17}$$

From equation (15) it follows that

$$s - s_0 = ku > kV. \tag{18}$$

By making use of (18) we investigate the sign of the numerator in equation (16),

$$s(s - s_0) - kV^2 > kV(s - V) > 0. \tag{19}$$

The last inequality holds because $s > u > V$, which follows in a straightforward manner from the above. Therefore, the physically acceptable solution for U_l is the one with the positive sign (plotted in figure 3),

$$U_l = \frac{s(s - s_0) - kV^2}{\sqrt{(s - s_0)^2 - k^2V^2}}. \tag{20}$$

3.2. *Radial particle velocity*

In order to find the corresponding particle velocity, we eliminate s from (20) by employing equation (15):

$$U_l = \frac{(s_0 + ku)u - V^2}{\sqrt{u^2 - V^2}}. \tag{21}$$

In terms of the radial component of the particle velocity, $u_r = \sqrt{u^2 - V^2}$,

$$U_l = ku_r + s_0\sqrt{1 + \left(\frac{V}{u_r}\right)^2} + (k - 1)\frac{V^2}{u_r}. \tag{22}$$

The solution of equation (22) for $u_r(t)$ is shown in figure 4 (the one-to-one mapping between U_l and t is given by (2)). This theoretical result is in agreement with computational results for the axisymmetric compressible Euler equations by Haller *et al.* (2002).

3.3. *Emergence of anomaly*

Figure 3 shows that after impact (far right) the contact line velocity decreases rapidly from a theoretically infinite value at $t = 0$ whereas the shock velocity remains almost

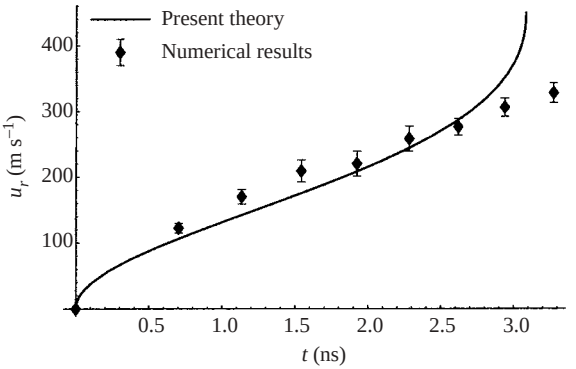

FIGURE 4. Prediction for the radial particle velocity and comparison with computational results.

constant. Later, (e.g. beyond $U_l = 7.5\,\mathrm{km\,s^{-1}}$) the shock velocity starts to grow, due to the development of lateral flow. However, after point A, where the tangent to the curve is parallel to the s-axis, the contact line velocity starts to increase again. This is a physically unacceptable situation and the solution branch above point A must be rejected. We conclude that there is a time after which no physical solution based on the assumed physics of a single shock wave attached to the contact line exists. The time corresponding to the point A will be termed as the 'time of shock degeneration', t_{deg}.

The jetting eruption in the contact line region, if it occurred before t_{deg}, would be the explanation of this anomaly. To address this issue, a closer look at the shock and contact line velocity corresponding to t_{deg} is needed. The maximum shock wave speed of the limit point A in figure 3 can be calculated from the condition

$$\frac{\partial U_l}{\partial s} = 0, \tag{23}$$

$$s_{max} = s_0 + V\left(\frac{2k-1}{3\beta}\alpha^{1/3} + \frac{\beta k}{\alpha^{1/3}}\right), \tag{24}$$

where the parameters α and β are defined as

$$\alpha = \frac{2kV}{s_0}, \quad \beta = \left(1 + \sqrt{1-\alpha^2\left(\frac{2k-1}{3k}\right)^3}\right)^{1/3}. \tag{25}$$

For the case of a linear fit for water, $s_{max} = 3.184\,\mathrm{km\,s^{-1}}$. At the same time, the contact line velocity has decreased to $U_{l,min} = 3.678\,\mathrm{km\,s^{-1}}$ (corresponding to the time $t_{deg} = 1.82\,\mathrm{ns}$). Obviously, $U_{l,min} > s$, hence, the jetting cannot be initiated at this time.

The interesting issue arising at this point is what happens to the shock envelope evolution in the time interval between t_{deg} and t_{jet} (for the numerical example of water used here, this is the interval [1.82 ns, 2.80 ns]). Due to the above-mentioned anomaly, the assumed single shock wave structure appears not to capture the physics correctly. We postulate the appearance of a double shock wave structure in this time interval, figure 5, which will remove the physically unacceptable portion of the earlier solution and lead to lateral jetting.

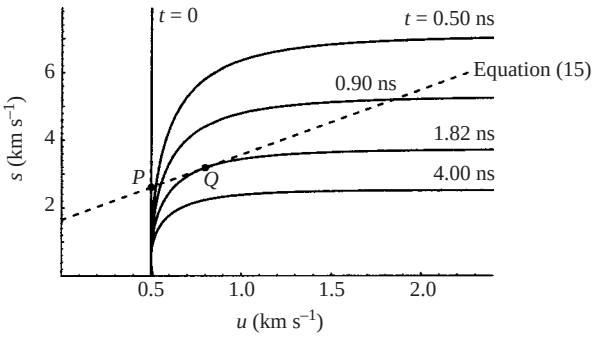

FIGURE 5. Construction of the solution: intersection of edge b.c. curves (each corresponding to a different time) and equation of state (straight line). No solution exists after $t = 1.82$ ns.

4. Solution of the anomaly

Additional insight into this anomaly is obtained by consideration of the process of solution construction in the contact line region, figure 5. The real flow state (u, s) is obtained as the intersection of the 'edge boundary condition' (henceforth referred to as 'edge b.c.') curves (14) and the linear Hugoniot fit (15). All edge b.c. curves originate from the same point $(V, 0)$, and rise sharply to a plateau value. The rise is less sharp as time increases. At each time instance, the linear Hugoniot fit and corresponding edge b.c. curve intersect at two points. However only the left point is physically acceptable, based on the following consideration. At time $t = 0$ the curves intersect at $u = 0.5$ (point P in figure 5) and $u \to \infty$. The first solution is the one we expect (no lateral flow, thus liquid velocity equal to the wall velocity). The solution $u \to \infty$ is physically not acceptable. Since the curve $u = u(t)$ must be continuous (no instantaneous acceleration of particles), all physically allowed solutions will travel from P to Q, figure 5.

Apparently, beyond $t = 1.82$ ns (marked with point Q in figure 5), no intersection exists. This is a different manifestation of the anomaly mentioned earlier. To explore this anomaly, we have to rethink the construction of the edge b.c. curves, since the linear Hugoniot has an overall validity (playing here the role of an equation of state). It is logical to assume that a somewhat more complex wave structure occurs and investigate its possible effect on the edge boundary curves.

Here, we consider a double wave structure, where the outer wave is assumed to be a shock wave, as outlined in figure 6. The liquid particle velocity in the region between the waves is still normal to the outer shock wave; however, the difference to the previous model (see equation (8)) is that it has a normal component $u_\perp$ smaller than the wall velocity V. Therefore we rewrite (8) as

$$\frac{\mathrm{d}l}{\mathrm{d}t} = a\frac{u}{u_\perp} = a\frac{u}{\lambda V}, \tag{26}$$

where we define the factor

$$\lambda = u_\perp / V \leqslant 1. \tag{27}$$

Implementing this concept in the solution process, equation (12) becomes

$$u(s) = \lambda\frac{V^2}{s}\left(1 + \frac{U_l}{a}\right). \tag{28}$$

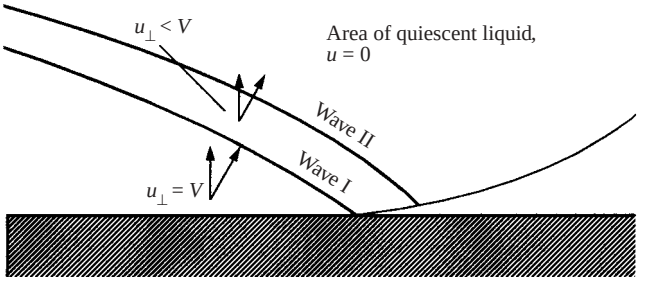

FIGURE 6. Schematic of a double wave structure in the contact line region.

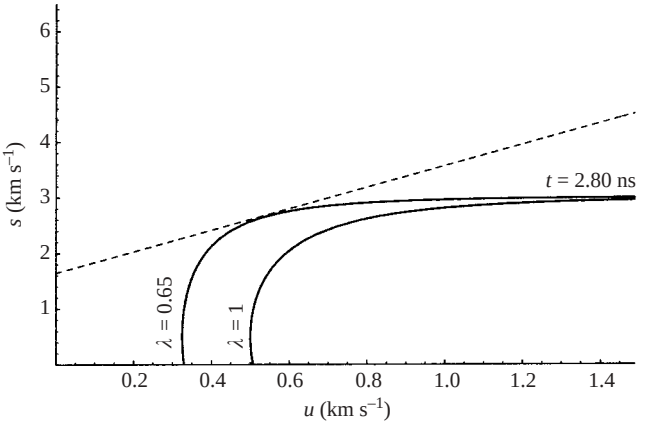

FIGURE 7. Effect of the factor λ on the edge b.c. curves allowing the existence of a solution up to the jetting time (here 1.82 ns).

Combining with equation (6) to eliminate a yields

$$u(s) = \lambda V \left(s + V\sqrt{1 - \frac{s^2 - V^2}{U_l^2}} \right) \Big/ \left(V + s\sqrt{1 - \frac{s^2 - V^2}{U_l^2}} \right). \tag{29}$$

Solving for the contact line velocity and recalling (15), equation (29) becomes

$$U_l(s) = \frac{s(s - s_0) - \lambda k V^2}{k\sqrt{u(s)^2 - \lambda^2 V^2}}. \tag{30}$$

The influence of the factor $\lambda < 1$ on the edge b.c. curves can be easily seen in equation (29). For the same value of s and U_l (corresponding to time t), the liquid velocity u will decrease with increasing λ. The curves in figure 7 clearly demonstrate the fact that in this scenario the domain of physically acceptable solutions is extended. For our example of a water droplet, the value of $\lambda = 0.65$ extends the range of acceptable solution up to $t = 2.80$ ns. This value coincides with the jetting time (for which $\sqrt{U_l^2 + V^2} = s$), thus removing the anomaly mentioned earlier.

Before closing this section, it is worth mentioning that a multiple wave structure (instead of only double) is also possible, since we have not made any assumption on the inner wave structure, which can be composed of different waves. Experiments (obviously very difficult to carry out) could define the exact wave structure present.

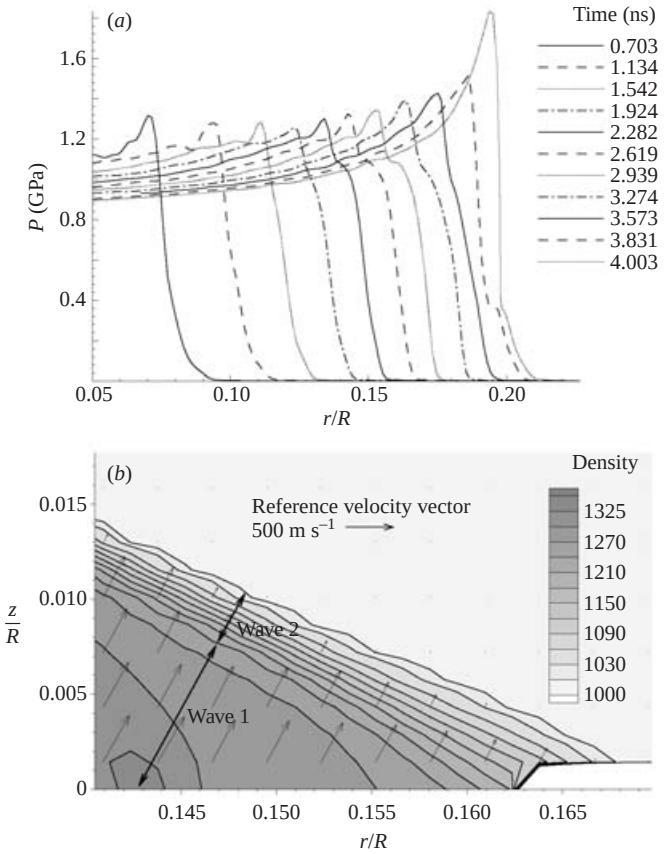

FIGURE 8. (*a*) Pressure wave profiles at the contact line in the radial direction for different times. Evidence of the single wave degeneration after $t \approx 1.5$ ns. (*b*) Equidistant iso-density lines.

Nevertheless, the proposed mechanism appears to offer a good explanation for the anomaly resulting from the single shock wave structure.

An equivalent argument could be also applied to the curve shown in figure 3, which would shift the point A together with the entire curve and extend the solution domain. However, the disadvantage of this approach would be that a specific function $\lambda = \lambda(t)$ (loss in generality), needs to be assumed.

5. Numerical confirmation

The proposed multiple wave structure, which allows the analytical treatment of the anomaly, was also numerically confirmed with the computational methodology outlined in Haller *et al.* (2002). No details are given here for brevity. The computations performed show the presence of the single shock wave up to the time of shock degeneration and subsequent gradual formation of a more complex wave structure in the contact line region.

The formation of the degenerated wave structure in terms of a numerically obtained pressure plot in the radial direction in the contact line area is examined in figure 8(*a*), showing clearly the breakup of the single shock wave after approximately $t = 1.5$ ns. Figure 8(*a*) clearly supports the double wave structure because it shows the pressure

distribution on the wall (at $z=0$) in the vicinity of the contact line and demonstrates that after some time a double wave structure occurs there (notice the distinctly different shape of the pressure distributions in this figure after the maximum pressure in each profile, for times greater than 1.924 ns).

The plots in figure 8(*b*) show the velocity field together with equidistant iso-density lines, confirming the assumption of lower velocity in the intermediate region, $\lambda < 1$. The narrow packing of equidistant iso-density lines indicate that the outer wave 2 is a shock wave (localized jump), with respect to which the particle velocity field is apparently normal. The factor λ, (27), with the numerically determined values in the region downstream of the shock wave was found to be 0.7.

A comment is also worthwhile regarding experimental confirmation of the mentioned multiple wave structure. To this end, the shock structure discussed in this work is outside the resolution capabilities of experimental techniques. Moreover, typical droplets used in experiments (Lesser & Field 1983; Field *et al.* 1989; Lesser 2002), are much bigger (droplet radii were 1–10 mm, i.e. 10–100 times bigger than in our simulation), which means also that the jetting times are much higher (since the contact line velocity as a function of time is also higher than for the smaller droplets, see Haller *et al.* 2002). Thus, a direct comparison with the configurations examined in our work is not easy to make.

6. Construction of the shock envelope

Based on the solution constructed above for the shock velocity, we develop an analytical representation for the shock envelope. This will be used to validate the shock–velocity model against numerical results obtained by Haller *et al.* (2002), since the shock velocity itself cannot be directly obtained from computations. The predicted shock velocity is evidently higher than the speed of sound, thus it is also expected that the shock envelope will differ substantially from the corresponding envelope in the acoustic limit, developed by Lesser (1981). We shall investigate the extent to which these two models differ and their agreement with computational results. The details of the numerical simulations can be found in Haller *et al.* (2002).

The procedure presented is a generalization of the acoustic approach by Lesser (1981) and regards the shock velocity as a solution of the Euler equations, therefore it can be used with an arbitrary equation of state.

We consider a contact line propagating to the right with the known radial velocity, $\dot{X}_l$. The coordinate system is shown in figure 9(*a*). The time coordinate is set to $t=0$ at the instant of impact. In our reference frame, the impact of a rigid wall with a perfect sphere of motionless liquid is investigated.

The contact line emits at $\tau \geqslant 0$ a circular wavelet spreading with the initial velocity $s(\tau)$, (figure 9*a*). The radius of the circular wave front at time t is

$$d(t,\tau) = \int_{\tau}^{t} s(\nu)\,\mathrm{d}\nu. \tag{31}$$

Let the coordinates of the spherical wave front at time t be (r, z) and those of the contact line at time τ, when the wave was emitted, $(X_l(\tau), V\tau)$. The equation of wavelets at time t in the (r, z)-plane will be

$$\Phi(r,z,\tau) = (r(t)-X_l(\tau))^2 + (z(t)-V\tau)^2 - d^2(t,\tau) = 0. \tag{32}$$

It is worth stressing that at each point on the constructed wave envelope only a single wavelet plays a role, hence this procedure does not employ any superposition of spatially overlapping wavelets (see also Lesser 1981). The velocity of these Huygens

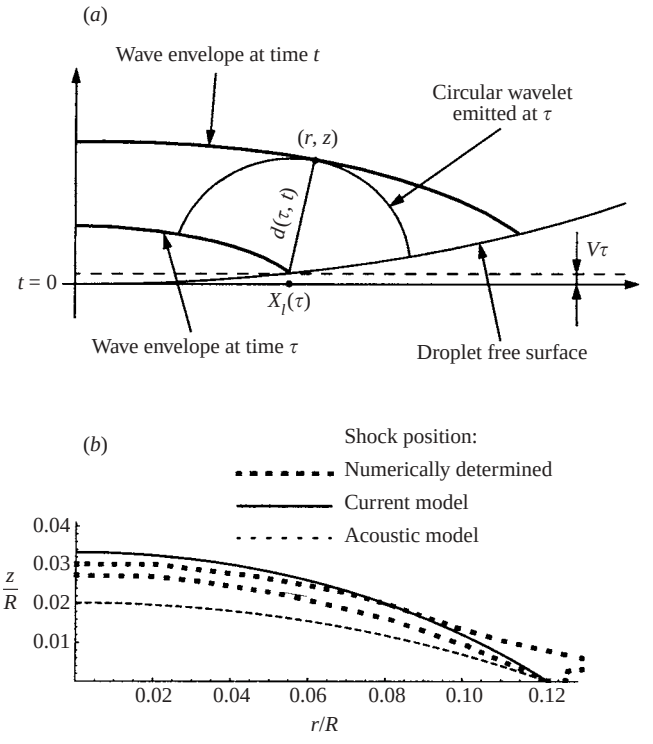

FIGURE 9. (*a*) Envelope construction: wall position at the time τ shown by a dashed line. Contact line propagates along the droplet free surface. (*b*) Comparison of analytical results with the computational findings.

wavelets is defined as the (highest) velocity at which the information (perturbation) travels into the undisturbed liquid, which is the shock speed. Next, we proceed with the construction of the wave front at specific time $t, t \geqslant \tau$, which we treat as a constant hereafter. To construct the envelope of the emitted wavelets (equation (32)), we project the surface $\Phi(r, z, \tau) = 0$ onto the (r, z)-plane (represented by the vector $(0, 0, 1)$) and require

$$\nabla\Phi(r, z, \tau) \cdot (0, 0, 1) = \frac{\partial}{\partial\tau}\Phi(r, z, \tau) = 0. \tag{33}$$

Insertion of (32) into (33) yields

$$\dot{X}_l(\tau)(r - X_l(\tau)) + V(z - V\tau) + d(\tau)\,\dot{d}\,(\tau) = 0. \tag{34}$$

From (31) it follows that

$$\dot{d}\,(\tau) = -s(\tau). \tag{35}$$

The physically meaningful solution of the system of equations (34) and (32), taking into account (35) is given in parametric form as

$$r(\tau) = X_l + \dot{d}\,(\tau)\frac{\dot{d}\,(\tau)\dot{X}_l(\tau) - V\sqrt{\dot{X}_l^2(\tau) + V^2 - s^2(\tau)}}{\dot{X}_l^2(\tau) + V^2}, \tag{36}$$

$$z(\tau) = V\tau + d(\tau)\frac{-\dot{d}\,(\tau)V + \dot{X}_l(\tau)\sqrt{\dot{X}_l^2(\tau) + V^2 - s^2(\tau)}}{\dot{X}_l^2(\tau) + V^2}. \tag{37}$$

The exact envelope functions (equations (36) and (37)) can be simplified by making use of the fact that during the first phase of the impact, the impact velocity V is much smaller than the contact line velocity $U_l = \dot{X}_l$,

$$V/\dot{X}_l \ll 1. \tag{38}$$

After implementation of (38) in (36) and (37),

$$r(\tau) \approx X_l(\tau) - d(\tau)\frac{s(\tau)}{U_l(\tau)}, \tag{39}$$

$$z(\tau) \approx V\tau - d(\tau)\sqrt{1 - \frac{s^2(\tau)}{U_l(\tau)}}. \tag{40}$$

Equations (39) and (40) are the parametric representation $r = r(\tau), z = z(\tau)$ of the shock envelope for small times t.

Up to this point, the approach is general and special solutions will depend on the function $s(\tau)$. The acoustic model (Lesser 1981) is a special case of the system (39)–(40) in the limit $s(\tau) = c$.

The exact function $s(\tau)$ can be obtained by equation (20). However, since this function is almost linear in the first impact phase (graph not included here for brevity), we approximate it with

$$s(\tau) = s_0 + \varepsilon\tau. \tag{41}$$

The value s_0 represents the initial shock velocity. Both s_0 and the coefficient ε can be obtained by the linearization of (20).

The radius $d(\tau)$ of the singular wavelet emitted at time τ, (31), is now

$$d(\tau) = \int_\tau^t (s_0 + \varepsilon\nu)\,\mathrm{d}\nu = s_0(t-\tau) + \frac{\varepsilon}{2}(t-\tau)^2 \tag{42}$$

Equations (41) and (42), when substituted into the system (39)–(40) yield the desired shock envelope in a parametric representation.

The comparison of the wave envelopes is shown in figure 9(*b*). The numerically captured shock position is contained within the two thick dashed lines. For the impact of a water droplet of 200 μm in diameter with the velocity $V = 500\,\mathrm{m\,s^{-1}}$, the linearization factor in equation (41) is $\varepsilon = 1.5 \times 10^{11}\,\mathrm{m\,s^{-2}}$. In the vicinity of the contact line region, the envelope developed matches the computational results well. The acoustic model, depicted by a thin dashed line, underpredicts the numerical findings, due to the underestimated envelope velocity in that model. Far from the contact line (near the z-axis), the computational envelope runs slightly below the position predicted by our model. This can be attributed to the temporal decay of the shock velocity, which is not included in the current model. Close to the contact line, this decay is negligible.

7. Conclusions

A model capable of predicting the liquid particle velocity and the shock speed in the compressed region of high-speed droplet impact on a solid surface is developed. The problem is resolved by taking into account the real equation of state. The analytical predictions of the model are in good agreement with computational results obtained by Haller *et al.* (2002). In the discussion of the first stage of droplet impact, it has been proven that the assumption of a single shock wave structure leads to the occurrence

of an anomaly in a contact line region. The present analysis shows that the anomaly does not emerge if a single-shock structure is not presupposed and more complex wave patterns are allowed. The assumption of multiple wave structure is validated by numerical results, showing the breakdown of the single-shock-wave assumption after the time of shock degeneration. The shock envelope generated upon impact is constructed and validated, showing good agreement with numerical findings.

REFERENCES

Cocchi, J. P. & Saurel, R. 1997 A Riemann problem based method for the resolution of compressible multimaterial flows, *J. Comput. Phys.* **137**, 265–298.

Field, J. E., Dear, J. P. & Ogren, J. E. 1989 The effects of target compliance on liquid drop impact. *J. Appl. Phys.* **65**, p. 533–540.

Field, J. E., Lesser, M. B. & Dear, J. P. 1985 Studies of two-dimensional liquid-wedge impact and their relevance to liquid drop impact problems. *Proc. R. Soc. Lond.* A **401**, 225–249.

Haller, K. K., Ventikos, Y., Poulikakos, D. & Monkewitz, P. 2002 A computational study of high-speed liquid droplet impact. *J. Appl. Phys.* **92**, 2821–2828.

Heymann, F. J. 1969 High-speed impact between a liquid drop and solid surface. *J. Appl. Phys.* **40**, 5113–5122.

Korobkin, A. 1992 Blunt-body impact on a compressible liquid surface. *J. Fluid Mech.* **244**, 437–453.

Korobkin, A. A. & Pukhnachov, V. V. 1988 Initial stage of water impact. *Annu. Rev. Fluid Mech.* **20**, 159–185.

Lesser, M. B. 1981 Analytic solutions of liquid-drop impact problems. *Proc. R. Soc. Lond.* A **377**, 289–308.

Lesser, M. B. 2002 The impact of compressible liquids. In *Droplet Surface Interactions* (ed. M. Rein). CISM Courses and Lectures No 456, International Centre for Mechanical Sciences, p. 101. Springer.

Lesser, M. B. & Field, J. E. 1974. The fluid mechanics of compressible liquid impact. In *Proc. 4th Intl Conf. on Rain Erosion and Associated Phenomena* (ed. A. A. Fyall & R. B. King), pp. 235–269. RAE, Farnborough, UK.

Lesser, M. B. & Field, J. E. 1983 The impact of compressible liquids. *Annu. Rev. Fluid Mech.* **15**, 97–122.

Rein, M. 1993 Phenomena of liquid drop impact on solid and liquid surfaces. *Fluid Dyn. Res.* **12**, 61–93.